Secondary Kinetics of Methanol Decomposition: Theoretical Rate Coefficients for $^3CH_2 + OH$, $^3CH_2 + {}^3CH_2$, and $^3CH_2 + CH_3$

Ahren W. Jasper,* Stephen J. Klippenstein,* and Lawrence B. Harding

Chemistry Division, Argonne National Laboratory, Argonne, Illinois 60439

Received: May 14, 2007; In Final Form: June 25, 2007

Direct variable reaction coordinate transition state theory (VRC-TST) rate coefficients are reported for the $^3CH_2 + OH$, $^3CH_2 + {}^3CH_2$, and $^3CH_2 + CH_3$ barrierless association reactions. The predicted rate coefficient for the $^3CH_2 + OH$ reaction ($\sim 1.2 \times 10^{-10}$ cm^3 molecule^{-1} s^{-1} for 300−2500 K) is 4−5 times larger than previous estimates, indicating that this reaction may be an important sink for OH in many combustion systems. The predicted rate coefficients for the $^3CH_2 + CH_3$ and $^3CH_2 + {}^3CH_2$ reactions are found to be in good agreement with the range of available experimental measurements. Product branching in the self-reaction of methylene is discussed, and the $C_2H_2 + 2H$ and $C_2H_2 + H_2$ products are predicted in a ratio of 4:1. The effect of the present set of rate coefficients on modeling the secondary kinetics of methanol decomposition is briefly considered. Finally, the present set of rate coefficients, along with previous VRC-TST determinations of the rate coefficients for the self-reactions of CH_3 and OH and for the $CH_3 + OH$ reaction, are used to test the geometric mean rule for the CH_3, $^3CH_2$, and OH fragments. The geometric mean rule is found to predict the cross-combination rate coefficients for the $^3CH_2 + OH$ and $^3CH_2 + CH_3$ reactions to better than 20%, with a larger (up to 50%) error for the $CH_3 + OH$ reaction.

I. Introduction

At temperatures and pressures relevant to combustion, the thermal dissociation of methanol produces $CH_3 + OH$ and $CH_2 + H_2O$ in a ratio of approximately 4:1,[1,2] and the secondary kinetics of methanol decomposition is therefore complicated by the presence of the reactive radicals methylene, methyl, and hydroxyl. For example, in a recent shock tube study[2] of the decomposition of CH_3OH, the modeled concentration of OH for some experimental conditions was found to be sensitive at intermediate and long times to the rate coefficients included in the reaction mechanism for

$$^3CH_2 + OH \rightarrow CH_2O + H \quad (1)$$

$$^3CH_2 + {}^3CH_2 \rightarrow C_2H_2 + 2H \quad (2a)$$

$$\rightarrow C_2H_2 + H_2 \quad (2b)$$

$$^3CH_2 + CH_3 \rightarrow C_2H_4 + H \quad (3)$$

The accuracy of the measured rates in that experimental study was therefore potentially limited by the accuracies of the available rate coefficients for reactions 1−3, and this concern is one motivation for the present theoretical study.

Despite the importance of CH_2 and OH in many combustion systems, their reaction (1) has not been well studied. The only measurement[3] of the rate coefficient for the $^3CH_2 + OH$ reaction (2.6×10^{-11} cm^3 molecule^{-1} s^{-1} at 1800−2300 K) is in good agreement with an earlier estimate of Tsang and Hampson,[4] whose recommendation was based on general arguments. Both determinations were assigned considerable uncertainty.

Several experimental studies of reactions 2 and 3 have been reported, but some ambiguities remain. For example, the two room-temperature determinations[5,6] of the rate for the self-reaction of methylene differ by a factor of 6, and, while two sets of experimental measurements[7−9] are in good agreement around 2000 K, the measured rates show qualitatively different temperature dependencies for 1000−2500 K. Furthermore, the $C_2H_2 + 2H$ and $C_2H_2 + H_2$ product channels have both been assigned as the dominant product channel, and their relative importance is not well understood.[10,11] Several room-temperature[12−15] and high-temperature[16−19] studies of the $^3CH_2 + CH_3$ reaction have appeared, with reported rate coefficients varying by as much as a factor of 5.

Accurate theoretical predictions of the rate coefficients for reactions 1−3 are not available, in part due to difficulties associated with computing rate coefficients for barrierless reactions. Variable reaction coordinate transition state theory[20−22] (VRC-TST) has been developed to treat barrierless reactions, and its direct implementation, in which the interaction potential of the reacting fragments is evaluated on-the-fly using multireference electronic structure calculations, allows for the efficient computation of quantitative rate coefficients. In recent studies[23,24] of systems with as many as eight carbon atoms, the VRC-TST method was shown to be computationally practical and to predict rate coefficients with estimated errors of less than 25% for a series of hydrocarbon radical−radical association reactions. The ab initio VRC-TST method was also recently used to describe the kinetics of the $CH_3 + OH$ association reaction with similar accuracy.[1] The main goal of the present Article is to study reactions 1−3 using ab initio VRC-TST.

The geometric mean rule[4,25,26] is an empirical that allows for the estimation of cross-combination rate coefficients from the self-recombination rates of the reacting partners. This rule has been shown to work remarkably well (to better than ∼20%) for a series of hydrocarbon radical−radical rate coefficients obtained using VRC-TST.[24] In the present work, the predicted rate coefficients for reactions 1−3, along with related previous

* Corresponding authors. E-mail: ajasper@sandia.gov and sjk@anl.gov.

10.1021/jp0736950 CCC: $37.00
Published on Web 08/15/2007

determinations[24,27] of the rate coefficients for the self-reactions of CH_3 and OH, are used to test the geometric mean rule for the $^3CH_2$, CH_3, and OH species.

In section II, details of the kinetics methods and electronic structure methods used are discussed. Results are presented in section III, and a test of the geometric mean rule is made in section IV. Section V is a summary.

II. Theory

II.A. Potential Energy Surfaces. In the VRC-TST rate calculations, the structures of the reacting fragments were kept fixed at their asymptotic equilibrium geometries, which were optimized at the B3LYP/6-311++G(d,p)[28,29] level of theory. The remaining degrees of freedom describe the relative orientation and separation of the fragments, and this interaction potential energy surface was treated as fully anharmonic and was computed on-the-fly using multireference perturbation theory[30] (CASPT2). The active space for the CASPT2 calculations was chosen to be the minimum required to correctly describe the separated fragments: four electrons in four orbitals for the $^3CH_2 + {}^3CH_2$ reaction, three electrons in three orbitals for the $^3CH_2 + CH_3$ reaction, and five electrons in four orbitals for the $^3CH_2 + OH$ reaction. For the $^3CH_2 + OH$ system, orbitals were optimized to minimize the average energy of the two lowest-energy states. A level shift[31] of 0.2 or 0.3 E_h (1 E_h = 627.5 kcal/mol) was applied in all of the CASPT2 calculations. The cc-pVDZ, aug-cc-pVDZ, and aug-cc-pVTZ Dunning basis sets[32,33] were used.

For reactions 2 and 3, a previously developed[24] basis set correction potential (BSCP) scheme was also considered. The BSCP is a one-dimensional energy correction that is a function of the forming C−C bond distance and is added to the CASPT2/cc-pVDZ interaction potential energy surface to approximate the result of a CASPT2/aug-cc-pVTZ-level calculation. This approach considerably reduces the computational expense of the electronic structure calculations, while retaining the accuracy of the larger basis set in the rate calculations. The BSCP was previously tested for several hydrocarbon association reactions,[24] where it was shown to predict the aug-cc-pVTZ basis set result for the self-reaction of CH_3 to better than 20%. In the present work, the BSCP scheme is tested for the methylene self-recombination reaction by comparing rate calculations using the BSCP scheme with those obtained using the aug-cc-pVTZ basis set directly. For the $^3CH_2 + CH_3$ reaction, a relatively large number of dividing surfaces was used to characterize the system, and the BSCP scheme was used to perform these calculations more efficiently.

For the $^3CH_2 + OH$ reaction, the spin−orbit splitting associated with the $^2\Pi$ state of the OH fragment was included as follows. Uncoupled energies for the two lowest-energy doublet states and the two lowest-energy quartet states were computed using state-averaged CASPT2 calculations and the active space and basis sets discussed above. Spin−orbit perturbations to the uncoupled energies were computed using state averaged CASSCF/6-311++G(d) wave functions and the Breit-Pauli operator,[34] and spin−orbit split energies were obtained by diagonalizing the resulting energy matrix. VRC-TST rate calculations for the $^3CH_2 + OH$ reaction in which spin−orbit splitting was neglected are also considered.

Although the focus of the present Article is the prediction of accurate capture rate coefficients for reactions 1−3, a brief discussion of possible competition between the various product channels is also presented. Channel energies were computed using B3LYP/6-311++G(d,p) geometries and QCISD(T)[35,36] energies extrapolated to the complete basis set (CBS) limit using the formula:[37]

$$E_{\mathrm{cc-pVxZ}} = E_{\mathrm{CBS}} + \frac{B}{(n_x + 1)^4} \tag{4}$$

where B is a fitting parameter, and $n_T = 3$ and $n_Q = 4$ for the cc-pVTZ and cc-pVQZ basis sets,[32] respectively. The Q_1 diagnostic,[38] which may be used to estimate the importance of multireference effects and thereby the reliability of the QCISD-(T) calculations, was found to be less than ~0.02 for all of the species considered, suggesting that the use of the QCISD(T) method is appropriate for these systems. Reaction enthalpies at 0 K were obtained using harmonic B3LYP/6-311++G(d,p) zero point energies and are summarized in Table 1, where they are compared with experimental values from a recent review[39,40] and from the online NIST database.[41] The QCISD(T)/CBS//B3LYP/6-311++G(d,p) energetics are in good agreement with the experimental results, with average errors of 0.5 and 1.3 kcal/mol for the Ruscic et al.[39,40] and NIST[41] experimental databases, respectively. This electronic structure theory method was tested[1] against accurate ATcT experimental results for CH_3OH and its associated bimolecular product channels and was found to have a root-mean-square error of only 0.3 kcal/mol for that system. The effect of using larger basis sets (cc-pVQZ and cc-pV5Z) to extrapolate to the complete basis set limit was tested for the $^3CH_2 + {}^3CH_2$ product channel energies, and the differences in the extrapolated thermochemistries were found to be less than 0.1 kcal/mol, on average.

The Gaussian program package[42] was used to perform the density functional theory calculations and geometry optimizations, and the Molpro program package[43] was used to perform the QCISD(T), CASPT2, and spin−orbit calculations.

II.B. Rate Calculations. Rate coefficients for the barrierless reactions were obtained using the VRC-TST method,[20−22] as implemented in the computer code VaReCoF.[44] In the VRC-TST method, nuclear motions are classified as either conserved or transitional modes,[45] where conserved modes correspond to the internal motions of the isolated fragments and transitional modes correspond to rigid fragment rotations and translations at large fragment separations and participate in bond formation, relative rotations, and overall rotation at intermediate distances. Conserved modes are assumed to evolve adiabatically along the reaction path, and they are treated as separable from one another and from the transitional modes; that is, fragment relaxation at finite fragment separations is neglected. The transitional modes, which typically have low frequencies and are highly anharmonic, are treated classically as fully anharmonic and coupled to one another. The flux for the transitional modes is obtained via Monte Carlo sampling, and the flux for the conserved modes is obtained using the harmonic oscillator approximation and frequencies set to those of the isolated fragments. This prescription allows for an efficient evaluation of the flux through transition state dividing surfaces appropriate for barrierless reactions, while retaining the most important mode−mode couplings and anharmonicities.

The geometry dependence of the optimal dividing surface for barrierless reactions may vary significantly as a function of total energy E, total angular momentum J, and temperature. In the present work, several types of dividing surfaces were considered, and the optimal dividing surface for each E,J pair was determined variationally. Thermal rate coefficients were then obtained by averaging over the microcanonically optimized fluxes with the appropriate Boltzmann weights.

TABLE 1: Reaction Enthalpies and Stationary Point Energies at 0 K (kcal/mol)

reaction	present[a]	experimental[b]	experimental[c]
$^3CH_2 + OH \rightarrow$			
CH_2OH	−104.58	−104.8 ± 0.4	−104.8 ± 1.1
CH_3O	−95.50	−95.5 ± 0.7	−97.0 ± 1.5
$CH_2O + H$	−75.90	−75.7 ± 0.4	−75.5 ± 1.0
trans-HCOH + H	−23.87	−23.7 ± 0.5	
cis-HCOH + H	−19.69	−19.0 ± 0.5	
$^2CH + H_2O$	−18.47	−17.7 ± 0.4	−17.2 ± 1.0
$^4CH + H_2O$	−0.86		
$[CH_2OH \leftrightarrow H_3CO]^‡$ (SP1)	−65.92		
$[^3CH_2 + OH \leftrightarrow {}^4CH + H_2O]^‡$ (SP2)	7.57		
$^3CH_2 + {}^3CH_2 \rightarrow$			
C_2H_4	−171.89	−172.2	−171.8 ± 1.4
$C_2H_2 + H_2$	−131.32	−132.1	−131.9 ± 1.4
$^3C_2H_4$	−106.30		
$C_2H_3 + H$	−62.73	−63.2	
$C_2H_2 + 2H$	−27.99	−28.8	−28.7 ± 1.4
$CH_3 + {}^2CH$	−9.88	−9.3 ± 0.6	−8.7 ± 1.4
$[C_2H_4 \leftrightarrow H_2CC + H_2]^‡$ (SP3)	−78.05		
$[^3C_2H_4 \leftrightarrow C_2H_3 + H]^‡$ (SP4)	−58.96		
$[C_2H_3 + H \leftrightarrow C_2H_2 + 2H]^‡$ (SP5)	−24.11		
$^3CH_2 + CH_3 \rightarrow$			
C_2H_5	−97.63		−100.7 ± 1.7
$C_2H_4 + H$	−62.65	−63.0	−62.8 ± 1.0
rms deviation	0.5,[d] 1.3[e]		

[a] QCISD(T)/CBS//B3LYP/6-311++G**. [b] Ruscic et al.[39,40] For the HCOH + H channels, energies were obtained by transforming the channel energies reported for $CH_3 + OH \rightarrow HCOH + H_2$ in ref 1 using heats of formation for CH_3, $^3CH_2$, and H from ref 39. [c] NIST online database.[41] [d] RMS deviation from the experimental values of Ruscic et al. [e] RMS deviation from the experimental values of the NIST database.

TABLE 2: VRC-TST Pivot Point Specifications

system	type of dividing surface	interfragment distances[a]
$^3CH_2 + OH$	CoM[b]	4.5(0.5)10, 11(2)15
$^3CH_2 + {}^3CH_2$	CoM	5(0.5)9, 10, 11(2)15
$^3CH_2 + CH_3$	CoM	4.5(0.5)9, 10, 11(2)15
	MF[c] $d = 0.5(0.5)2.0$	4(0.5)9, 10, 11(2)15

[a] *X*(*Y*)*Z* denotes a grid of distances from *X* to *Z* in steps of *Y*. [b] Pivot points located at the centers of mass of both fragments. [c] Multifacted variable reaction coordinate dividing surfaces with pairs of pivot points displaced from the methyl radical C atom by the distance *d*.

The sets of transition state dividing surfaces used in the VRC-TST calculations for reactions 1−3 are summarized in Table 2. For all three reactions, center of mass (CoM) dividing surfaces were used, where these dividing surfaces are defined in terms of a fixed CoM separation of the reacting fragments. CoM dividing surfaces are expected to be appropriate at low temperatures, where centrifugal barriers at large fragment separations are the dynamical bottlenecks for association.

At higher temperatures, the dominant centrifugal barriers occur at shorter fragment separations where chemical bonding begins to take place, and variable reaction coordinate (VRC) dividing surfaces are generally more appropriate. When multiple sites are available for bonding, multifaceted (MF) VRC dividing surfaces, described in detail elsewhere,[46] are required. VRC and MF dividing surfaces are obtained by defining one or more pivot point locations for each fragment around which the fragment is allowed to rotate rigidly. The pivot points need not be located at an atomic center or at the center of mass of the fragment. For radical−radical reactions, pivot points are typically displaced from the atom participating in bond formation along the singly occupied orbital. A minimum separation for each pair of pivot points located on different fragments is then defined, and the overall dividing surface is obtained by considering geometries that do not violate any of the minimum separation criteria and that have at least one pivot point separation equal to its minimum allowed value. The resulting dividing surface is continuous and may therefore be variationally optimized with respect to the fragment separation and the location of the pivot points.

For the methylene fragment, VRC dividing surfaces with pivot points displaced from the carbon atom out of the plane of the $^3CH_2$ molecule and displaced along the C_2 axis of $^3CH_2$ were considered but were found to not be important in characterizing the transition state for these reactions. For the methyl radical, the use of MF VRC dividing surfaces with pivot points displaced from the carbon atom perpendicular to the plane of CH_3 was found to reduce the computed rate coefficients by as much as 10%, and such surfaces were included.

The VRC-TST rate calculations were corrected for dynamical recrossing using the transmission coefficient obtained in a previous trajectory study[24] of hydrocarbon radical−radical association reactions. This value was found to be 0.85 and independent of temperature.

Rovibronic coupling (i.e., the angular momentum coupling of the electronic and rotational degrees of freedom) has a significant effect on the total partition function of the reactant OH, especially at low temperatures. For transition state species at sufficiently large fragment separations, the effect of rovibronic coupling may be expected to be similar to that of OH, whereas, for shorter fragment separations, the effect of rovibronic coupling is less clear. This coupling is neglected in the VRC-TST calculations, and, if we assume that the effect of rovibronic coupling at the transition state is similar to that for the reactant OH, it is appropriate to neglect rovibronic coupling when computing the partition function for OH. We chose to treat the electronic partition function for OH classically and as uncoupled to rotation in a previous study[1] of the $CH_3 + OH$ reaction, and good agreement was obtained with experimental results for that system.

We briefly consider two processes with finite barriers: the $OH + {}^3CH_2 \rightarrow {}^4CH + H_2O$ abstraction reaction, and the $C_2H_4 \rightarrow H_2CC + H_2$ fragmentation reaction. The rate coefficients for these reactions were obtained using rigid rotor/harmonic oscillator variational transition state theory with energies obtained at the QCISD(T)/CBS level of theory along the B3LYP/6-311++G(d,p) minimum energy paths and using B3LYP/6-311++G(d,p) frequencies. The lowest-frequency

TABLE 3: Capture Rate Coefficients Fit to $A(T/298\ \mathrm{K})^n \exp(-E/T)$ for $T = 300-2500$ K

reaction	A (cm^3 molecule^{-1} s^{-1})	n	E (K)
$^3CH_2 + OH$	9.545×10^{-11}	0.1228	−81.43
$^3CH_2 + OH^a$	1.418×10^{-13}	2.019	3410
$^3CH_2 + {}^3CH_2$	1.491×10^{-10}	0.0022	4.460
$^3CH_2 + CH_3$	2.821×10^{-10}	−0.3432	77.05

[a] Direct abstraction on the quadruplet surface.

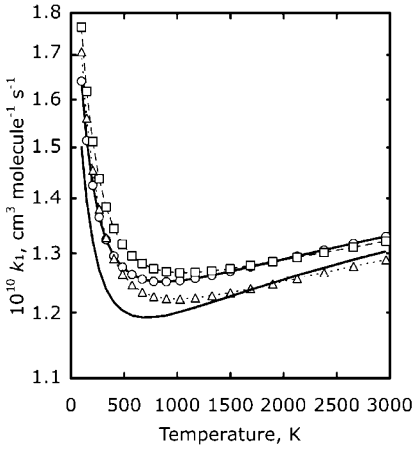

Figure 1. Dynamically corrected VRC-TST rate coefficients for the $^3CH_2 + OH$ reaction without spin−orbit splitting for the cc-pVDZ (△), aug-cc-pVDZ (□), and aug-cc-pVTZ (○) basis sets and with spin−orbit splitting for the aug-cc-pVTZ basis set (−).

mode in the OH + $^3CH_2$ reaction was treated as a hindered rotor with a period of 360° and a rotational barrier of 2.3 kcal/mol. Polyrate[47] was used to compute the minimum energy paths for these two processes and to compute projected vibrational frequencies along the minimum energy paths using Cartesian coordinates.

III. Results and Discussion

The best present theoretical prediction of the rate coefficient for the reactions discussed in this section was fit to a modified Arrhenius expression, and the results are summarized in Table 3.

III.A. $^3CH_2$ + OH. Dynamically corrected VRC-TST rate coefficients for the $^3CH_2 + OH$ reaction were computed using the CASPT2 method and the cc-pVDZ, aug-cc-pVDZ, and aug-cc-pVTZ basis sets, and the results are shown in Figure 1. The predicted rate coefficients show very little basis set dependence, differing from one another by less than 6% over the temperature range 300−2500 K. The orientation-dependent spin−orbit splitting correction was found to decrease the predicted rate coefficient for the aug-cc-pVTZ basis set by only 7% at room temperature and to have less of an effect at higher temperatures. The incorporation of spin−orbit splitting was previously shown to have a similarly minor effect on the VRC-TST rate coefficient for the $CH_3 + OH$ association reaction.[1]

The $^3CH_2 + OH$ reaction proceeds via the energized adduct CH_2OH^*, whose lowest-energy pathway for fragmentation (as shown in Table 1) is the formation of $H + CH_2O$. This process is exothermic by 75 kcal/mol, and the energy of the $H + CH_2O$ product channel is only 35 kcal/mol higher than the energy of the CH_2OH complex, suggesting that k_1 is independent of pressure at conditions relevant to combustion. The energized adduct may also decay via loss of either H atom from the methylene group, but these product channels are significantly higher in energy (∼55 kcal/mol) than the formaldehyde product channel. Isomerization of the energized adduct to CH_3O is also possible. The energy of methoxy radical is 9 kcal/mol higher than the energy of CH_2OH, and the barrier to isomerization is 39 kcal/mol.

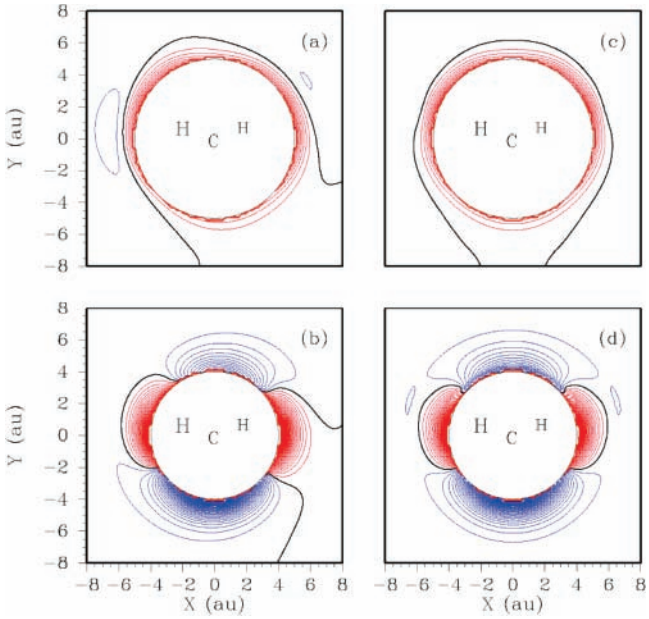

Figure 2. CASPT2/aug-cc-pVDZ interaction energies for the first (b and d) and second (a and c) doublet states of $^3CH_2 + OH$, shown as a function of Cartesian displacements (X and Y, 1 au = 0.529 Å) of the O atom away from the C atom in the plane of methylene. The hydroxyl H atom is either in the plane (a and b) or perpendicular to it (c and d), and the C−O−H bond angle is 90°. Energies are defined relative to the separated fragments, the contour spacing is 1 kcal/mol, and black, red, and blue contours denote zero, positive, and negative energies, respectively.

The abstraction reaction

$$^3CH_2 + OH \rightarrow {}^4CH + H_2O \qquad (5)$$

takes place on the quartet surface and has a zero-point-inclusive forward barrier height of 7.6 kcal/mol. The rate coefficient for this process was computed using variational transition state theory and the rigid rotor and harmonic oscillator approximations, as discussed in section II. The predicted rate coefficient for abstraction is more than 10 times slower than the rate coefficient for reaction 1 at 2500 K, and the relative importance of the abstraction reaction rapidly decreases at lower temperatures.

The importance of abstraction on the doublet surface was also considered. In Figure 2, cuts through the first and second CASPT2/aug-cc-pVDZ doublet surfaces of $^3CH_2 + OH$ are shown for geometries where the O atom is in the plane of the methylene fragment. The hydroxyl H atom is either in the plane (panels a and b) or perpendicular to it (panels c and d), and the C−O−H bond angle is 90°. The ground electronic state (Figure 2b and d) shows a large attractive region near the σ_v plane of methylene leading to the formation of CH_2OH. The shallow wells in Figure 2d located near the C−H bonds are evidence of hydrogen bonding, and there is no evidence of a saddle point for hydrogen atom abstraction on the doublet surface. We may conclude that the dominant product channel of reaction 1 is $CH_2O + H$ via the association/dissociation mechanism discussed above.

Tsang and Hampson[4] estimated the rate coefficient for the $^3CH_2 + OH$ reaction to be 3×10^{-11} cm^3 molecule^{-1} s^{-1}, independent of temperature and pressure, with an uncertainty

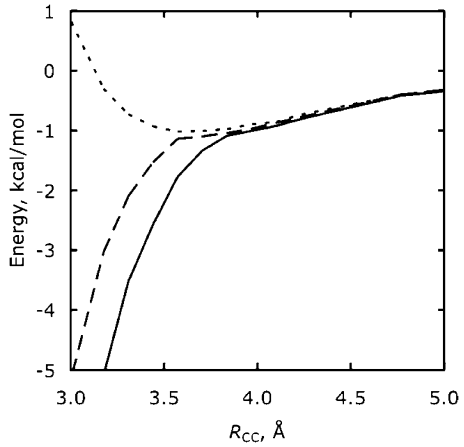

Figure 3. Minimum energy path for the $^3CH_2 + {}^3CH_2$ association reaction on the singlet (solid), triplet (dashed), and quintet (dotted) surfaces computed using the CASPT2/aug-cc-pVDZ method.

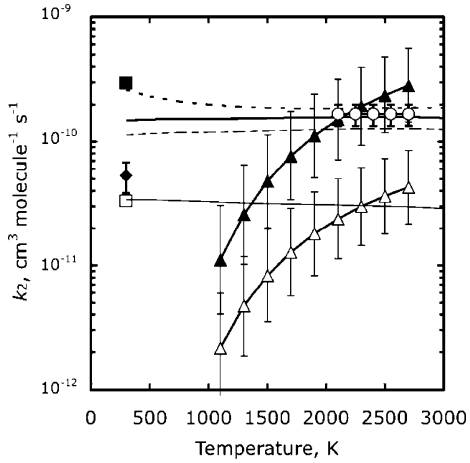

Figure 4. Rate coefficient for the $^3CH_2 + {}^3CH_2 \rightarrow C_2H_2 + H_2$ (thin solid) and $C_2H_2 + 2H$ (thin dashed) reactions and their total (thick solid). The statistically coupled total rate coefficient, including contributions from the quintet surface, is shown as a thick dotted line. Also shown are the experimental rate coefficients of Braun et al.[5] (diamond), Frank et al.[7,8] (circles), Carstensen[6] (squares), and Bauerle et al.[9] (triangles), where open and filled symbols denote the $C_2H_2 + H_2$ and $C_2H_2 + 2H$ products, respectively.

factor of 3 for 300−2500 K. A similar value ($2.6 \pm 1.6 \times 10^{-11}$ cm^3 molecule^{-1} s^{-1} at 1900−2170 K and ∼1 atm) was obtained in a shock tube study[3] of reaction 1, and the experiments were found to be difficult to interpret at temperatures above 2170 K, presumably due to the increased importance of secondary reactions. The present value of $\sim 1.2 \times 10^{-10}$ cm^3 molecule^{-1} s^{-1} is 4−5 times larger than these previous values. This significant adjustment in the rate coefficient for the $^3CH_2 +$ OH reaction is important for understanding the long-time kinetics of methanol decomposition, as discussed in section III.D.

III.B. $^3CH_2 + {}^3CH_2$. Self-recombination of triplet methylene may proceed on the singlet and triplet electronic surfaces, as shown in Figure 3. The quintet surface is not reactive but is attractive for fragment separations greater than ∼3 Å. VRC-TST rate coefficients were variationally optimized for the singlet and triplet surfaces separately (i.e., the singlet and triplet surfaces were assumed to be electronically adiabatic or uncoupled from one another) and summed to obtain a total rate coefficient for the self-reaction of $^3CH_2$. The triplet surface is somewhat less attractive than the singlet surface along the minimum energy path for association, and the rate coefficient for the triplet surface is a factor of 2.1−2.5 greater than that for the singlet surface, when the electronic degeneracy factors are included.

For the temperature range 300−2500 K, the total rate coefficient computed using the cc-pVDZ basis set is ∼25% lower than that obtained using the aug-cc-pVTZ basis set, while the rate coefficients computed using the aug-cc-pVDZ and aug-cc-pVTZ basis sets differ by less than 5%. The rate coefficient computed using the BSCP scheme accurately reproduces the aug-cc-pVTZ result, differing by only ∼10% over the temperature range considered. The total rate coefficient computed using the aug-cc-pVTZ basis set is $\sim 1.5 \times 10^{-10}$ cm^3 molecule^{-1} s^{-1} for 300−2500 K, as shown in Figure 4.

The reactive flux for association on the quintet surface was computed using VRC-TST, but, due to the nonreactive region of the surface at short fragment separations, the variationally optimized reaction rate is predicted to be zero. One could artificially restrict the set of dividing surfaces considered in the variational optimizations to those in the attractive region of the interaction potential, but the resulting rate coefficient would be meaningful only at very low temperatures. Instead, we estimate the maximum contribution of the quintet surface to the overall rate coefficient for the $^3CH_2 + {}^3CH_2$ reaction by variationally optimizing the geometry of the dividing surface with respect to the sum of the fluxes computed for the singlet, triplet, and quintet surfaces. We refer to this as the "statistically coupled" model, which may be compared with the electronically adiabatic model discussed above.

This statistically coupled model predicts a rate coefficient that is larger than the adiabatic rate coefficient by a factor of 2 at room temperature and by only ∼20% at temperatures above 1500 K, as shown in Figure 4. The statistically coupled model gives an upper bound on the effect of the quintet surface on the total rate coefficient, with the lower bound given by the uncoupled rate coefficient. Despite the ambiguity at low temperatures, we may conclude that the effect of the quintet surface is likely to be small at temperatures relevant to combustion. Elsewhere in this Article, we restrict our attention to the adiabatic prediction for the rate coefficient with the quintet surface neglected, unless otherwise noted.

The singlet−triplet gap in isolated methylene is 9 kcal/mol,[39] and the theoretical characterization of reaction 1 is therefore complicated by the presence of singlet methylene at elevated temperatures. At 2500 K, for example, more than 10% of equilibrated methylene is in the singlet state, and the $^3CH_2 + {}^1CH_2$ reaction may be estimated to make up ∼25% of methylene−methylene collisions. Asymptotically, the $^3CH_2 + {}^1CH_2$ fragments correlate electronically with the second triplet state of the reactive system, and preliminary calculations suggest that, at large fragment separations, the minimum energy path for association on this surface is relatively more attractive than that for the self-recombination of triplet methylene on the ground-state triplet surface. At a C−C distance of ∼3 Å, the characters of the two triplet states become mixed, and an electronic transition to the ground-state triplet surface is required for the $^3CH_2 + {}^1CH_2 \rightarrow C_2H_4$ reaction to proceed, which could reduce the rate coefficient for this process at intermediate and high temperatures. Despite this ambiguity, the rate coefficient for the $^3CH_2 + {}^1CH_2$ reaction may be larger than that for triplet methylene self-recombination on the triplet surface due to differences in the electronic partition functions of the reactants, which could have a measurable effect in some experimental situations at high temperatures. A more detailed discussion of the rate for the $^3CH_2 + {}^1CH_2$ reaction requires consideration of the competition between association and intersystem crossing and is beyond the scope of the present work.

Next, product branching in the $^3CH_2 + {}^3CH_2$ reaction is discussed. The formation of the energized adduct C_2H_4* is exothermic by 172 kcal/mol, and several product channels are available, as shown in Table 1. The lowest-energy pathway for fragmentation is the loss of H_2, which proceeds via a saddle point (SP3) with a zero-point-inclusive energy of −78 kcal/mol relative to the reactants, corresponding to a barrier height of 94 kcal/mol. This transition state has previously been characterized[48] using multireference configuration interaction (MR-CI) calculations, which are in good agreement with the present QCISD(T)/CBS//B3LYP/6-311++G(d,p) results. The loss of H_2 via SP3 initially produces H_2CC, which then quickly isomerizes over a low barrier to form acetylene.

The energized complex may also barrierlessly lose an H atom to form $C_2H_3 + H$, which has a channel energy of −63 kcal/mol relative to reactants or 109 kcal/mol relative to C_2H_4. The loss of H initially produces internally excited C_2H_3, and this product likely quickly decays (perhaps even prior to collisions) by loss of another H atom to give $C_2H_2 + 2H$, particularly at elevated temperatures where C_2H_3 is not readily stabilized. Although this channel is 15 kcal/mol higher in energy than the $H_2 + H_2CC$ saddle point, the "loose" transition state region for the barrierless loss of H has a higher density of states than the "tight" transition state associated with the loss of H_2. Both processes may therefore be important at the energies produced by the $^3CH_2 + {}^3CH_2$ reaction.

The $CH_3 + CH$ channel is also exothermic relative to $^3CH_2 + {}^3CH_2$. This product channel is significantly higher in energy than the $C_2H_2 + H_2$ and $C_2H_2 + 2H$ product channels and is unlikely to be a significant product.

Competition between channels 2a and 2b is studied using a three-channel ($^3CH_2 + {}^3CH_2$, $H_2CC + H_2$, and $C_2H_3 + H$) model. As discussed above, methylene association may take place on both the singlet and the triplet surfaces, and we characterize the entrance channel using the total VRC-TST microcanonical fluxes discussed above, which include contributions from both the singlet and the triplet surfaces. We then make the assumption that once the system passes through the dynamical bottleneck for association on the triplet surface the resulting complex quickly decays to singlet C_2H_4, and the competition between the two product channels is therefore independent of the initial electronic state and may be modeled by considering competition on the singlet electronic suface. In this model, the triplet C_2H_4 complex is not considered.

One could also treat the triplet surface as completely uncoupled from the singlet surface and consider the product branching for the singlet and triplet C_2H_4* complexes independently. The dissociation of triplet C_2H_4 has been previously characterized theoretically,[49] and in that study no saddle point for H_2 loss on the triplet surface was found and the exclusive decay channel was shown to be the formation of $H + C_2H_3$. The latter process has only a small barrier on the triplet surface,[49] as shown in Table 1. The uncoupled model for product branching in the $^3CH_2 + {}^3CH_2$ reaction will therefore predict the formation of significantly more $H + C_2H_3$, and this prediction may be regarded as an upper limit, as it is unlikely that the dynamics of the singlet and triplet surfaces are uncoupled during the reactive event. We will return to this model briefly below.

The transition state for the $H_2 + H_2CC$ channel on the singlet surface was treated using rigid rotor/harmonic oscillator variational transition state theory, as discussed in section II. The $H + C_2H_3$ product channel on the singlet surface was previously characterized[23,48] using VRC-TST, and a very similar treatment was followed in the present work.

Stabilization is not an important process at pressures considered here (up to at least 10^5 Torr), and, in the low-pressure limit, the microcanonical branching probability for channel α is given by

$$P_\alpha(E,J) = N_\alpha / \sum_{\alpha'} N_{\alpha'} \tag{6}$$

where $N_\alpha(E,J)$ is the microcanonical flux for channel α. Thermally averaged rate coefficients for the individual product channels may be readily obtained from eq 6, and thermally averaged product branching probabilities are then given by

$$P_\alpha(T) = k_\alpha / \sum_{\alpha'} k_{\alpha'} \tag{7}$$

This treatment is equivalent to a low-pressure-limit master equation simulation, and the calculations were performed using Variflex.[50]

For 300−2500 K, the present theoretical treatment predicts $P_{2b} = 0.19-0.23$, with the remainder of the rate attributed to $C_2H_3 + H$. At elevated temperatures, C_2H_3 readily dissociates to $C_2H_2 + H$, and we may interpret $P_{H + C_2H_3}$ as the probability of forming $C_2H_2 + 2H$, that is, as P_{2a}. The $C_2H_2 + 2H$ and $C_2H_2 + H_2$ products are therefore predicted in a ratio of ∼4:1 and independent of pressure and only very weakly dependent on temperature. (At high enough pressures where stabilization of the C_2H_4 complex can occur, product branching will be pressure dependent. Our calculations suggest that stabilization of the complex is not important at pressures up to at least 10^5 Torr.) We note that if the singlet and triplet surfaces are treated as uncoupled and the triplet C_2H_4 complex is assumed to decay exclusively to $C_2H_2 + 2H$, the product branching ratio is increased to 14:1, which may be regarded as an upper limit. A more complete treatment of the coupling between the singlet and triplet electronic surfaces is beyond the scope of this article.

Figure 4 shows the dynamically corrected total VRC-TST rate coefficient (k_2), the product specific rate coefficients (k_{2a} and k_{2b}) from eq 7, and several experimental results. There have been two experimental determinations[5,6] at room temperature, and these results differ by a factor of 6. The VRC-TST result at room temperature (1.5×10^{-10} cm^3 molecule^{-1} s^{-1}) is intermediate of the two experimental results (0.5 and 3.3×10^{-10} cm^3 molecule^{-1} s^{-1} in refs 5 and 6, respectively). It is interesting to note that the statistically coupled model, which includes the maximum contribution from the quintet surface, predicts a rate coefficient at room temperature that is in close agreement with the measured rate coefficient of Carstensen.[6]

At 2000−3000 K, the magnitude of the VRC-TST rate coefficient is in good agreement with available experimental results[7−9] and is somewhat higher than the results of ref 9 for 1100−2000 K. The VRC-TST rate coefficient predicts no temperature dependence, in agreement with the experimental results of Frank et al.,[7,8] but in contrast to the significant temperature dependence observed by Bauerle et al.[9]

At 298 K, Braun et al.[5] assigned $C_2H_2 + H_2$ (2b) as the dominant product, which agrees with the assignment of Carstensen.[6] Walsh and co-workers[10,11] later argued that Braun et al.'s value should be reinterpreted as the rate for $C_2H_2 + 2H$ (2a), and this interpretation was supported by several modeling studies. A similar controversy occurs at high temperatures, where Frank et al.[7,8] assigned their measured rate to $C_2H_2 + 2H$, whereas, in a more recent study of reaction 2, Bauerle et

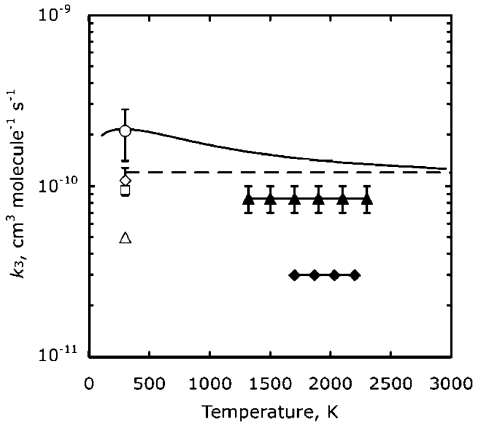

Figure 5. Rate coefficient for the $^3CH_2 + CH_3 \rightarrow C_2H_4 + H$ reaction (−). Also shown are the experimental results of Laufer and Bass[13] (□), Pilling and Robertson[12] (△), Bhaskaran et al.[18] (◆), Frank and Braun-Unkhoff[16] (▲), Deters et al.[14] (◇), and Wang and Fockenberg[15] (○), as well as the recommended value of Baulch et al.[53] (dashed line).

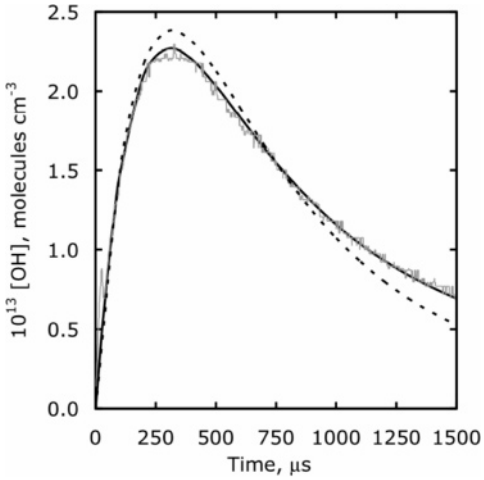

Figure 6. Observed [OH] profile (gray) for one of the experimental measurements reported in ref 2. Also shown are the modeled profiles obtained using the improved reaction mechanism (solid) and using the previous value for k_1 and with reactions 2 and 3 removed from the reaction mechanism (dotted). The conditions for this profile are $T =$ 1925 K, $P_1 = 10.92$ Torr, $M_s = 2.802$, $\rho_5 = 2.291 \times 10^{18}$ molecules cm^{-3}, and $[CH_3OH]_0 = 5.475 \times 10^{13}$ molecules cm^{-3}.

al.[9] observed $C_2H_2 + 2H$ and $C_2H_2 + H_2$ in a ratio of approximately 1:6. As discussed above, the present analysis predicts a temperature-independent branching ratio of ∼4:1 for the $C_2H_2 + 2H$ and $C_2H_2 + H_2$ channels.

The present set of theoretical predictions for the product branching in the self-reaction of triplet methylene may be compared with a recent experimental[51] study of the photolysis of ethylene at 157 nm. This photon energy (182 kcal/mol) is close to the channel energy of $^3CH_2 + {}^3CH_2$ relative to C_2H_4, and one may compare the fragmentation dynamics of photoexcited and thermally energized ethylene complexes. In the photolysis experiments, the $C_2H_2 + 2H$ and $C_2H_2 + H_2$ products were observed with probabilities of 0.7 and 0.3, respectively. The photolysis of ethylene at 157 nm was also modeled[52] using RRKM theory, with the $C_2H_2 + 2H$ and $C_2H_2 + H_2$ products predicted with probabilities of 0.6 and 0.4, respectively. The present theoretical results for product branching in the bimolecular reaction are in qualitative agreement with these results.

III.C. $^3CH_2 + CH_3$. VRC-TST calculations of the capture rate coefficient for the $CH_3 + {}^3CH_2$ reaction were carried out for temperatures from 300−2500 K using the CASPT2 method and the cc-pVDZ and aug-cc-pVDZ basis sets. For the temperature range considered, the rate coefficient computed using the cc-pVDZ basis set is 30−40% lower than the aug-cc-pVDZ rate coefficient. The rate coefficient computed using the BSCP scheme is in good agreement with the aug-cc-pVDZ result.

Figure 5 shows the VRC-TST rate coefficient computed using the BSCP along with several experimental results. The present value is in excellent agreement with the most recent room-temperature determination[15] (2.1×10^{-10} cm^3 molecule^{-1} s^{-1}). Three earlier determinations[12−14] at room temperature are 25−50% of the present value. As discussed in detail elsewhere,[15] the reported rate coefficient for the $^3CH_2 + CH_3$ reaction is sensitive to the rate for

$$CH_3 + CH_3 \rightarrow \text{products} \qquad (8)$$

and the use of a consistent value for k_8 when analyzing the experimental results brings the measured value of Deters et al.[14] in excellent agreement with that of Wang and Fockenberg.[15] We note that in ref 15, k_8 was measured to be $4.6 \pm 1.0 \times 10^{-11}$ cm^3 molecule^{-1} s^{-1}, which may be compared with the results of a recent VRC-TST calculation[24] (5.8×10^{-11} cm^3 molecule^{-1} s^{-1}). The two other room-temperature measurements relied on reaction mechanisms that may have been incomplete, as suggested elsewhere.[15]

At elevated temperatures, the VRC-TST rate coefficient shows a weak negative temperature dependence and is approximately twice the measured value of Frank and Braun-Unkhoff[16] (8.5×10^{-11} cm^3 molecule^{-1} s^{-1} for 1300−2300 K) and 5 times the value of Bhaskaran et al.[18] (3×10^{-11} cm^3 molecule^{-1} s^{-1} for 1700−2200 K), both of which were obtained from shock tube measurements. Modeling studies[17,19] at elevated temperatures have also suggested the use of lower values than the one predicted here. The recommended value of Baulch et al.[53] was obtained by averaging the four room-temperature experimental results and assuming a temperature-independent rate.

III.D. Secondary Kinetics of Methanol Decomposition. The present set of theoretical rate coefficients was previously used as part of a larger reaction mechanism to fit observed OH absorption profiles in shock tube studies of the decomposition of methanol.[2] In these studies, the rate coefficient for CH_3OH decomposition and the branching ratio for the $CH_3 + OH$ and $CH_2 + H_2O$ products were measured by monitoring OH formation and loss. OH loss occurs by reaction with methyl radical, methylene, and hydroxyl radical (and, at low temperatures, by reaction with CH_3OH), and the measured CH_3OH decomposition rate coefficient and product branching ratio were found to be sensitive to the values of the rate coefficients included in the reaction mechanism for these reactions.

As discussed in ref 2, at some temperatures the use of the previous, lower value for k_1 (2.6×10^{-11} cm^3 molecule^{-1} s^{-1}) resulted in poor fits of the observed [OH] at intermediate and long times. The reaction mechanism was modified to include the present predicted value for k_1, which is 5 times larger than the previous estimate, as well as reactions 2 and 3 and the $^3CH_2 + H$ reaction. The resulting reaction mechanism was found to be capable of fitting the observed OH traces out to long times for a range of experimental conditions. This is illustrated for one set of experimental conditions in Figure 6, where an OH absorption profile from ref 2 at 1925 K is shown along with the fit obtained using the improved reaction mechanism, where only the rate coefficient for CH_3OH decomposition and the CH_3OH product branching ratio were adjusted to fit the observed

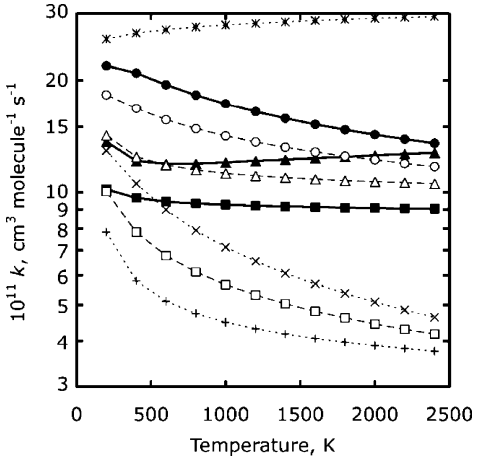

Figure 7. Rate coefficients for the $^3CH_2 + CH_3$ (circles), $^3CH_2 + OH$ (triangles), and $CH_3 + OH$ (squares) reactions calculated using VRC-TST (filled symbols) and estimated using the geometric mean rule (open symbols). Also shown are the self-recombination rate coefficients ($\times 2$) for CH_3 ($\times$), OH (+), and $^3CH_2$ (*).

[OH] profile. Agreement between the observed and fitted profiles is excellent. Furthermore, the resulting measured rate coefficient and product branching ratio for CH_3OH decomposition were found to be in good agreement with theoretical predictions.[1,2]

Also shown in Figure 6 is the effect of using the previous value for the rate coefficient for the $^3CH_2 + OH$ reaction and excluding the reactions of $^3CH_2$ with $^3CH_2$, CH_3, and H from the reaction mechanism. These changes significantly degrade the quality of the fit, demonstrating the importance of these reactions at these conditions. Furthermore, the two reaction mechanisms predict qualitatively different behaviors at long times such that simply reoptimizing the rate coefficient for CH_3OH decomposition and the product branching ratio does not significantly improve the quality of the fit using the previous reaction mechanism.

IV. Test of the Geometric Mean Rule for $^3CH_2$, CH_3, and OH

The geometric mean rule relates the self-recombination rate coefficients for two reacting partners (k_A and k_B) to their cross-combination rate coefficient k_{AB} by

$$k_{AB} = 2\sqrt{k_A k_B} \tag{9}$$

In section III, the cross-combination rate coefficients for the $^3CH_2 + CH_3$ and $^3CH_2 + OH$ reactions and the self-recombination rate coefficient for $^3CH_2$ were obtained using the VRC-TST method. Previously, VRC-TST rate coefficients for the self-recombination of methyl radical[24] and hydroxyl radical[27] as well as for the $CH_3 + OH$ reaction[1] were obtained. The VRC-TST rate coefficients for the $CH_3 + OH$ and $CH_3 + CH_3$ reactions were shown[1,24] to agree well with available experimental results, and the rate for the self-recombination of hydroxyl radical is in excellent agreement with the statistical adiabatic channel model (SACM) determination of Troe and Ushakov.[54] This set of six accurate VRC-TST rate coefficients allows for a systematic study of the accuracy of the geometric mean rule for the $^3CH_2$, CH_3, and OH fragments, and the results are shown in Figure 7.

For the $^3CH_2 + OH$ reaction, the estimated and calculated rate coefficients are in excellent agreement and differ by less than ~15%. The estimated rate coefficient for the $^3CH_2 + CH_3$ reaction is systematically lower than the calculated rate coefficient, but the error in the estimated rate coefficient is still only ~20%. Errors of this magnitude are in agreement with previous tests[24] of the geometric mean rule for the CH_3, C_2H_5, *tert*-C_4H_9, and iso-C_3H_7 fragments using VRC-TST rate coefficients.

As seen in Figure 7, the geometric mean rule is accurate for the $CH_3 + OH$ reaction at room temperature but has an error of as much as a factor of 2 at elevated temperatures. The rate coefficients for the OH and CH_3 self-recombination reactions both show significant negative temperature dependences (and, therefore, so does the rate coefficient for the $CH_3 + OH$ reaction estimated by the geometric mean rule), whereas the calculated $CH_3 + OH$ rate coefficient is nearly independent of temperature. Several factors may contribute to the temperature dependence of the rate coefficients shown in Figure 7. The most important factor for the OH + OH reaction is the ratio of the electronic partition function for the transition state to the product of the electronic partition functions for the reactants, which (if the electronic partition function for OH is treated independently of nuclear rotation and is therefore given by $2 + 2\exp(-139\ \text{cm}^{-1}/k_BT)$) varies from ~1/9 to ~1/15 over the temperature range 300−2500 K. The electronic partition function factor for CH_3 self-recombination is independent of temperature and is 1/4, and the geometric mean rule (which effectively models the electronic partition function factor for the cross reaction as the geometric mean of the electronic partition functions for the self-reactions) correctly treats the temperature dependence of the electronic partition function factor for the cross combination reaction (giving 1/6−1/8 for 300−2500 K).

Excluding the electronic partition function, the calculated rate coefficient for OH self-recombination shows a slight negative temperature dependence, and the $CH_3 + OH$ reaction shows a slight positive temperature dependence. These behaviors are consistent with dipole−dipole and dipole−induced-dipole long-range forces, respectively.[55] The CH_3 self-recombination reaction is dominated by dispersion forces at long range, which would suggest a positive temperature-dependent rate coefficient. However, the calculated rate coefficient decreases rapidly by a factor of 3 over the temperature range 300−2500 K. This significant decrease is due to the increased importance of steric repulsions of the reacting methyl radical fragments as the dynamical bottleneck moves to shorter fragment separations at elevated temperatures. Steric effects would not be expected to be significant for the OH self-recombination reaction, but it is perhaps surprising that they are not observed in the $CH_3 + OH$ reaction. They may be partially offset for this reaction by the relatively strong interaction energy of the $CH_3 + OH$ reaction. Regardless, the geometric mean rule appears to overpredict the importance of steric repulsions in the $CH_3 + OH$ reaction and thus significantly underestimates the rate coefficient for this reaction at elevated temperatures.

V. Conclusions

Rate coefficients for the $^3CH_2 + OH$, $^3CH_2 + {}^3CH_2$, and $^3CH_2 + CH_3$ barrierless association reactions were computed using variable reaction coordinate transition state theory coupled with direct multireference perturbation theory electronic structure calculations, and the results are summarized in Table 3. For the $^3CH_2 + OH$ reaction, the predicted rate coefficient is 4−5 larger than previous estimates, and this value is shown to be important for accurately modeling the intermediate and long time kinetics of methanol decomposition. The predicted rate coefficients for the $^3CH_2 + {}^3CH_2$ and $^3CH_2 + CH_3$ reactions are in good agreement with the range of experimental results and may be used to differentiate between experimental measure-

ments when discrepancies exist. Product branching in the self-recombination of triplet methylene was also considered, and the present analysis suggests that $C_2H_2 + 2H$ and $C_2H_2 + H_2$ are formed in a ratio of 4:1.

The geometric mean rule was tested for the CH_3, $^3CH_2$, and OH fragments and was found to be very accurate for the $^3CH_2 + OH$ and $^3CH_2 + CH_3$ reactions. Errors in the geometric mean rule for these reactions were less than 20%, which are similar in magnitude to errors observed in an earlier test of the geometric mean rule for saturated hydrocarbon radicals. The geometric mean rule was found to perform less well for the $CH_3 + OH$ reaction, with errors as large as a factor of 2.

Acknowledgment. We thank J. V. Michael and N. K. Srinivasan for encouraging these calculations and for providing data from their shock tube experiments for Figure 6. This work was performed under the auspices of the Office of Basic Energy Sciences, Division of Chemical Sciences, Geosciences, and Biosciences, U.S. Department of Energy, under contract number DE-AC02-06CH11357.

References and Notes

(1) Jasper, A. W.; Klippenstein, S. J.; Harding, L. B.; Ruscic, B. *J. Phys. Chem. A* **2007**, *111*, 3932.

(2) Srinivasan, N. K.; Su., M.-C.; Michael, J. V. *J. Phys. Chem. A* **2007**, *111*, 3951.

(3) Krasnoperov, L. N.; Michael, J. V. *J. Phys. Chem. A* **2004**, *108*, 8317.

(4) Tsang, W.; Hampson, R. F. *J. Phys. Chem. Ref. Data* **1986**, *15*, 1087.

(5) Braun, W.; Bass, A. M.; Pilling, M. J. *J. Chem. Phys.* **1970**, *52*, 5131.

(6) Carstensen, H. H. Dissertation, Max-Planck-Institut für Strömungsforschung, Göttingen, 1995.

(7) Frank, P.; Just, T. *Proc. Int. Symp. Shock Tubes Waves* **1984**, *14*, 706.

(8) Frank, P.; Bhaskaran, K. A.; Just, T. *J. Phys. Chem.* **1986**, *90*, 2226.

(9) Bauerle, S.; Klatt, M.; Wagner, H. G. *Ber. Bunsen-Ges. Phys. Chem.* **1995**, *99*, 870.

(10) Frey, H. M.; Walsh, R. *J. Phys. Chem.* **1995**, *89*, 2445.

(11) Becerra, R.; Canosa-Mas, C. E.; Frey, H. M.; Walsh, R. *J. Chem. Soc., Faraday Trans. 2* **1987**, *83*, 435.

(12) Pilling, M. J.; Robertson, J. A. *J. Chem. Soc., Faraday Trans. 1* **1977**, *73*, 968.

(13) Laufer, A. H.; Bass, A. M. *J. Phys. Chem.* **1974**, *78*, 1344.

(14) Deters, R.; Ottig, M.; Wagner, H. G.; Temps, F.; Dóbé, S. *Ber. Bunsen-Ges. Phys. Chem.* **1998**, *102*, 978.

(15) Wang, B.; Fockenberg, C. *J. Phys. Chem. A* **2001**, *105*, 8449.

(16) Frank, P.; Braun-Unkhoff, M. *16th Int. Symp. Shock Tubes Waves* **1987**.

(17) Olsen, D. B.; Gardiner, W. C. *Combust. Flame* **1978**, *32*, 152.

(18) Bhaskharan, K.; Frank, P.; Just, T. *12th Int. Symp. Shock Tubes Waves* **1979**.

(19) Hidaka, Y.; Sato, K.; Henmi, Y.; Tanaka, H.; Inami, K. *Combust. Flame* **2000**, *118*, 340.

(20) Klippenstein, S. J. *J. Chem. Phys.* **1992**, *96*, 367.

(21) Klippenstein, S. J. *J. Phys. Chem.* **1994**, *98*, 11459.

(22) Georgievskii, Y.; Klippenstein, S. J. *J. Chem. Phys.* **2003**, *118*, 5442.

(23) Harding, L. B.; Georgievskii, Y.; Klippenstein, S. J. *J. Phys. Chem. A* **2005**, *109*, 4646.

(24) Klippenstein, S. J.; Georgievskii, Y.; Harding, L. B. *Phys. Chem. Chem. Phys.* **2006**, *10*, 1133.

(25) Kerr, J. A.; Trotman-Dickenson, A. F. *Prog. React. Kinet.* **1961**, *1*, 105.

(26) Blake, A. R.; Henderson, J. F.; Kutschke, K. O. *Can. J. Chem.* **1961**, *39*, 1920.

(27) Jasper, A. W.; Klippenstein, S. J., unpublished.

(28) Becke, A. D. *J. Chem. Phys.* **1993**, *98*, 5648. Lee, C.; Yang, W.; Parr, R. G. *Phys. Rev. B* **1998**, *37*, 785.

(29) Krishnan, R.; Binkley, J. S.; Seeger, R.; Pople, J. A. *J. Chem. Phys.* **1980**, *72*, 650. Clark, T.; Chadrasekhar, J.; Schleyer, P. v. R. *J. Comput. Chem.* **1993**, *4*, 294.

(30) Andersson, K.; Malmqvist, P.-A.; Roos, B. O. *J. Chem. Phys.* **1992**, *96*, 1218. Werner, H.-J. *Mol. Phys.* **1996**, *89*, 645. Celani, P.; Werner, H.-J. *J. Chem. Phys.* **2000**, *112*, 5546.

(31) Roos, B. O.; Andersson, K. *Chem. Phys. Lett.* **1995**, *245*, 215. Celani, P.; Werner, H.-J. *J. Chem. Phys.* **2003**, *119*, 5044.

(32) Dunning, T. H., Jr. *J. Chem. Phys.* **1989**, *90*, 1007.

(33) Kendall, R. A.; Dunning, T. H., Jr.; Harrison, R. J. *J. Chem. Phys.* **1992**, *96*, 6796.

(34) Berning, A.; Schweizer, M.; Werner, H.-J.; Knowles, P. J.; Palmier, P. *Mol. Phys.* **2000**, *98*, 1823.

(35) Pople, J. A.; Head-Gordon, M.; Raghavachari, K. *J. Chem. Phys.* **1987**, *87*, 5968. Raghavachari, K.; Trucks, G. W.; Pople, J. A.; Head-Gordon, M. *Chem. Phys. Lett.* **1989**, *157*, 479.

(36) The ROHF-RQCISD(T) algorithm is used for the open shell QCISD(T) calculations. See: Knowles, P. J.; Hampel, C.; Werner, H.-J. *J. Chem. Phys.* **1993**, *99*, 5219; **2000**, *112*, 3106(E).

(37) Martin, J. M. L.; Uzan, O. *Chem. Phys. Lett.* **1998**, *282*, 16.

(38) Lee, T. J.; Rendell, A. P.; Taylor, P. R. *J. Phys. Chem.* **1990**, *94*, 5463.

(39) Ruscic, B.; Boggs, J. E.; Burcat, A.; Császár, A. G.; Demaison, J.; Janoschek, R.; Martin, J. M. L.; Morton, M. L.; Rossi, M. J.; Stanton, J. F.; Szalay, P. G.; Westmoreland, P. R.; Zabel, F.; Bérces, T. *J. Phys. Chem. Ref. Data* **2005**, *34*, 573.

(40) Burcat, A.; Ruscic, B. "Third Millennium Ideal Gas and Condensed Phase Thermochemical Database for Combustion with updates from Active Thermochemical Tables" TAE # 960; ANL-50/20 Technion-IIT, Aerospace Engineering, and Argonne National Laboratory, Chemistry Division, 2005.

(41) NIST Computational Chemistry Comparison and Benchmark Database, NIST Standard Reference Database Number 101 Release 12, August 2005, Johnson, R. D., III, Ed.; http://srdata.nist.gov/cccbdb.

(42) Frisch, M. J.; Trucks, G. W.; Schlegel, H. B.; Scuseria, G. E.; Robb, M. A.; Cheeseman, J. R.; Montgomery, J. A., Jr.; Vreven, T.; Kudin, K. N.; Burant, J. C.; Millam, J. M.; Iyengar, S. S.; Tomasi, J.; Barone, V.; Mennucci, B.; Cossi, M.; Scalmani, G.; Rega, N.; Petersson, G. A.; Nakatsuji, H.; Hada, M.; Ehara, M.; Toyota, K.; Fukuda, R.; Hasegawa, J.; Ishida, M.; Nakajima, T.; Honda, Y.; Kitao, O.; Nakai, H.; Klene, M.; Li, X.; Knox, J. E.; Hratchian, H. P.; Cross, J. B.; Bakken, V.; Adamo, C.; Jaramillo, J.; Gomperts, R.; Stratmann, R. E.; Yazyev, O.; Austin, A. J.; Cammi, R.; Pomelli, C.; Ochterski, J. W.; Ayala, P. Y.; Morokuma, K.; Voth, G. A.; Salvador, P.; Dannenberg, J. J.; Zakrzewski, V. G.; Dapprich, S.; Daniels, A. D.; Strain, M. C.; Farkas, O.; Malick, D. K.; Rabuck, A. D.; Raghavachari, K.; Foresman, J. B.; Ortiz, J. V.; Cui, Q.; Baboul, A. G.; Clifford, S.; Cioslowski, J.; Stefanov, B. B.; Liu, G.; Liashenko, A.; Piskorz, P.; Komaromi, I.; Martin, R. L.; Fox, D. J.; Keith, T.; Al-Laham, M. A.; Peng, C. Y.; Nanayakkara, A.; Challacombe, M.; Gill, P. M. W.; Johnson, B.; Chen, W.; Wong, M. W.; Gonzalez, C.; Pople, J. A. *Gaussian 98*, revision A.7; Gaussian, Inc.: Wallingford, CT, 2004.

(43) Werner, H.-J.; Knowles, P. J.; Lindh, R.; Manby, F. R.; Schütz, M.; Celani, P.; Korona, T.; Rauhut, G.; Amos, R. D.; Bernhardsson, A.; Berning, A.; Cooper, D. L.; Deegan, M. J. O.; Dobbyn, A. J.; Eckert, F.; Hampel, C.; Hetzer, G.; Lloyd, A. W.; McNicholas, S. J.; Meyer, W.; Mura, M. E.; Nicklass, A.; Palmieri, P.; Pitzer, R.; Schumann, U.; Stoll, H.; Stone A. J.; Tarroni, R.; Thorsteinsson, T. MOLPRO, Version 2006.1.

(44) Georgievskii, Y.; Klippenstein, S. J. VaReCoF, Sandia National Laboratories and Argonne National Laboratory, 2006.

(45) Wardlaw, D. M.; Marcus, R. A. *Chem. Phys. Lett.* **1984**, *110*, 230; *J. Chem. Phys.* **1985**, *83*, 3462; *J. Phys. Chem.* **1986**, *90*, 5838.

(46) Georgievskii, Y.; Klippenstein, S. J. *J. Phys. Chem. A* **2003**, *107*, 9776.

(47) Corchado, J. C.; Chuang, Y.-Y.; Fast, P. L.; Hu, W.-P.; Liu, Y.-P.; Lynch, G. C.; Nguyen, K. A.; Jackels, C. F.; Fernandez Ramos, A.; Ellingson, B. A.; Lynch, B. J.; Melissas, V. S.; Villà, J.; Rossi, I.; Coitiño, E. L.; Pu, J.; Albu, T. V.; Steckler, R.; Garrett, B. C.; Isaacson, A. D.; Truhlar, D. G. POLYRATE, version 9.4, University of Minnesota, Minneapolis, 2005.

(48) Klippenstein, S. J.; Harding, L. B. *Phys. Chem. Chem. Phys.* **1999**, *1*, 989.

(49) Kim, G.-S.; Nguyen, T. L.; Mebel, A. M.; Lin, S. H.; Nguyen, M. T. *J. Phys. Chem. A* **2003**, *107*, 1788.

(50) Klippenstein, S. J.; Wagner, A. F.; Dunbar, R. C.; Wardlaw, D. M.; Robertson, S. H.; Miller, J. A. Variflex, version 1.14m, Argonne National Laboratory, 2006.

(51) Lee, S.-H.; Lee, Y. T.; Yang, X. *J. Chem. Phys.* **2004**, *120*, 10983.

(52) Chang, A. H. H.; Mebel, A. M.; Yang, X.-M.; Lin, S. H.; Lee, Y. T. *Chem. Phys. Lett.* **1998**, *287*, 301; *J. Chem. Phys.* **1998**, *109*, 2748.

(53) Baulch, D. L.; Bowman, C. T.; Cobos, C. J.; Cox, R. A.; Just, Th.; Kerr, J. A.; Pilling, M. J.; Stocker, D.; Troe, J.; Tsang, W.; Walker, R. W.; Warnatz. J. *J. Phys. Chem. Ref. Data* **2005**, *34*, 757.

(54) Troe, J.; Ushakov, V. G. *Phys. Chem. Chem. Phys.*, submitted.

(55) Georgievskii, Y.; Klippenstein, S. J. *J. Chem. Phys.* **2005**, *122*, 194103.